Inorganic Chemistry Communications 129 (2021) 108646

Contents lists available at ScienceDirect

Inorganic Chemistry Communications

journal homepage: www.elsevier.com/locate/inoche

Short communication

A systematic influence of Cu doping on structural and opto-electrical properties of fabricated Yb_2O_3 thin films for Al/Cu-Yb_2O_3/p-Si Schottky diode applications

K.S. Mohan [a], A. Panneerselvam [b,*], R. Marnadu [c], J. Chandrasekaran [c], Mohd. Shkir [d], A. Tataroğlu [e]

[a] Department of Physics, Nandha Engineering College (Autonomous), Erode 638 052, Tamil Nadu, India
[b] Department of Physics, Vivekanandha College of Engineering for Women (Autonomous), Elayampalayam, Tiruchengode, Namakkal 637 205, Tamil Nadu, India
[c] Department of Physics, Sri Ramakrishna Mission Vidyalaya College of Arts and Science (Autonomous), Coimbatore 641 020, Tamil Nadu, India
[d] Advanced Functional Materials & Optoelectronics Laboratory, Department of Physics, College of Science, King Khalid University, Abha 61413, Saudi Arabia
[e] Department of Physics, Faculty of Science, Gazi University, Ankara, Turkey

ARTICLE INFO

Keywords:
Rare earth metal oxides
Yb_2O_3
JNSP method
MIS Schottky diode
Optical and electrical properties

ABSTRACT

In the present work, transition metal doped rare earth metal oxide (Cu-Yb_2O_3) thin films have been effectively synthesized on a large scale using low-cost jet nebulizer spray pyrolysis (JNSP) route at different copper (Cu) doping concentrations (0, 1.5, 2.5, 3.5, and 4.5 wt%) with optimized substrate temperature of 550 °C. The structural, morphological and opto-electrical properties were investigated using various characterization techniques. The X-ray diffraction (XRD) profile indicates the polycrystalline nature of all the deposited films with a cubic phase and the size of crystallites is found to increase from 11 to 31 nm. The field emission scanning electron microscope (FESEM) images reveal that the Cu doping has significant impact on the surface morphology of Cu-Yb_2O_3 films. The atomic force microscope (AFM) analysis exposed higher roughness value for 4.5 wt% of Cu-Yb_2O_3 films. The elemental composition study approves the presence of Yb, Cu and O in the film. The transmittance and indirect optical energy gap of Cu-Yb_2O_3 films have been analyzed by UV–Visible spectroscopy which established the systematic band gap reduction of Yb_2O_3 thin films from 3.68 to 3.14 eV with increasing Cu concentrations. The DC electrical studies showed a maximum conductivity and minimum average activation energy for 4.5 wt% of Cu-Yb_2O_3 film. The electrical characteristics of the fabricated Al/Cu-Yb_2O_3/p-Si Schottky diode was investigated using current–voltage (I-V) measurements performed under dark and light conditions. The Φ_B (0.911 eV in dark & 0.754 eV in illumination) and minimum n values (2.120 in dark and 1.757 in illuminations) were obtained for MIS diode having Cu doping concentration of 4.5 wt% in Yb_2O_3.

1. Introduction

In recent trend, most popular and very effective electronic devices such as metal-insulator-semiconductor (MIS) Schottky diode (SD)/ Schottky barrier diode (SBD), photodiode, UV photodetector have become most favorable when compared to other layered devices like metal–insulator-metal (MIM), metal-polymer-semiconductor (MPS) and metal–oxidesemiconductor (MOS). Especially, the MIS SDs contain excellent electrical behavior compared to other devices. The MIS SDs have unique features such as low forward voltage drop values, fast switching speed and high operating frequency [1–3]. Besides, the SDs have active role in various applications like radio frequency generator, optical communication system and microelectronic devices such as diode, transistor, capacitors and power conversion system [4–5]. Performance of MIS devices depends on several factors including the existence of an interfacial layer and interface states [6]. An interlayer of greater thickness may affect the device related parameters such as barrier height (Φ_B), ideality factor (n) and series resistance (R_s). Moreover, the MIS device becomes more popular in variation to the other types of SBDs because of their multifaceted applications [7–8].

Nowadays, rare earth metal oxides such as ytterbium trioxide (Yb_2O_3), neodymium trioxide (Nd_2O_3), samarium trioxide (Sm_2O_3) and

* Corresponding author.
E-mail address: panneer.phy@gmail.com (A. Panneerselvam).

https://doi.org/10.1016/j.inoche.2021.108646
Received 3 March 2021; Received in revised form 26 April 2021; Accepted 29 April 2021
Available online 4 May 2021
1387-7003/© 2021 Elsevier B.V. All rights reserved.

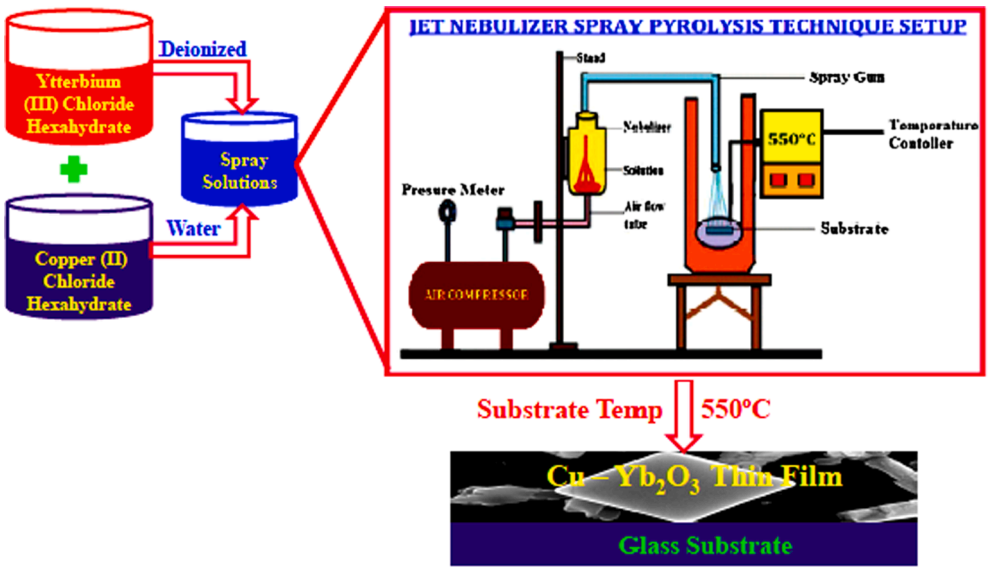


Fig. 1. Schematic illustration of JNSP technique and Cu-Yb_2O_3film growth process.

erbium trioxide (Er_2O_3) are important materials having good transparency, insulating coating and semiconducting properties. These materials have excellent optical, photoluminescence and electrical properties. Furthermore, they are used as an insulating layer in various devices such as MIS SDs and MOS capacitors due to their dielectric properties. Among them, the Yb_2O_3 is a suitable material for MIS diodes due to wide band gap (>4eV), low resistivity, optical absorption and insulating properties [9]. The dopants in the Yb_2O_3 lattice efficientlyamend the crystal distortions, oxygen vacancies and energy states. This change affects its optical and electrical properties. Especially, the dopant like Cu is perfect cationic dopant for Yb_2O_3as the atomic radii of Cu are relatively smaller compared to Yb [10–11].

Many researchers have attempted to investigate the electrical nature of p-Si SBDs via different metallization schemes. Marnadu *et. al.* studied the electrical characteristics of Cu/WO_3/p-Si SD by varying the Ni doping concentration and documented a high ideality factor for MIS diodes. Vivek *et. al* studied the electrical behavior of as deposited Cu/Ba-MoO_3/p-Si Schottky diodes and showed that the ideality factor varies from 5.40 to 3.09 and the barrier height increases from 0.62 to 0.72 eV from I-V characteristics. Balaji *et. al* reported that the fabricated Ni-MoO_3/p-Si diodes show a barrier height change from 0.75 to 0.83 eV and ideality factor can be increased to 2.03 [12–14]. However,

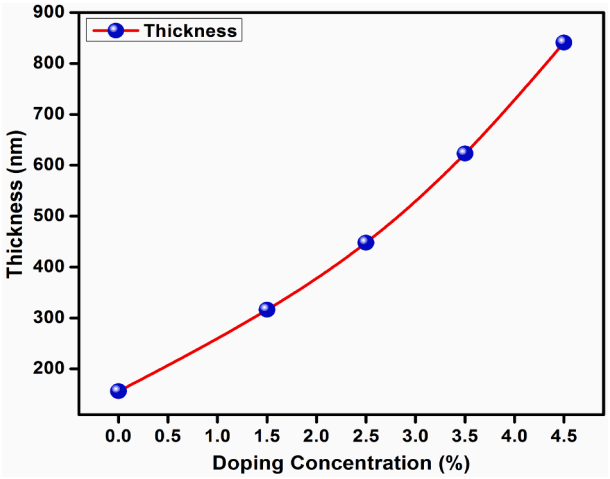


Fig. 2. Thickness variation of the Cu-Yb_2O_3 thin films for different doping concentrations.

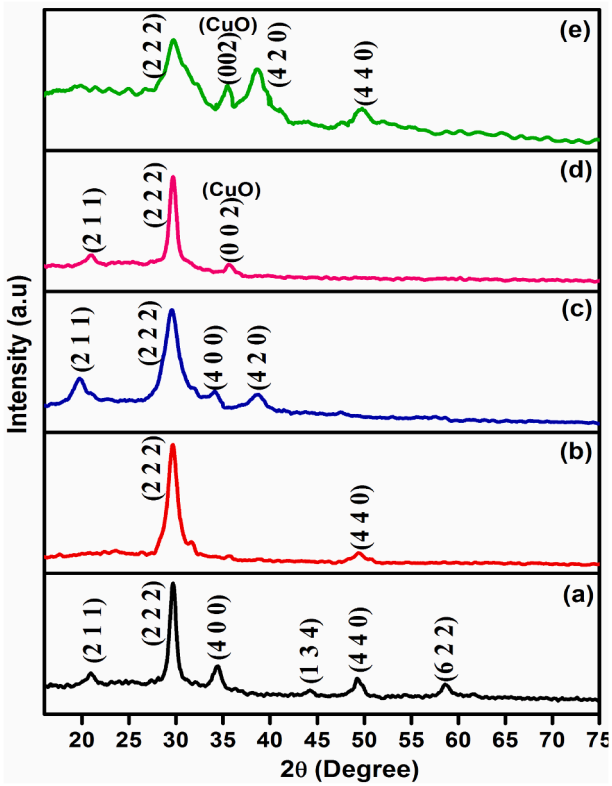


Fig.3. XRD pattern of the Cu-Yb_2O_3 thin films for different doping concentrations of (a) 0 wt%, (b) 1.5 wt%, (c) 2.5 wt% (d) 3.5 wt% and (e) 4.5 wt%.

compared to these results the rare earth metal oxides enhance the electrical conductivity. Moreover, the many Schottky contact materials such as Cu, Ag, Te, Au and Al exhibit good rectification behavior. The barrier height is considered to bereliant on voltage owed to the existence of an interlayer and the interfacial states. Furthermore, with low resistance and smaller bandgap Al offers a supreme Schottky connection with higher work function compared to other materials [15]. In the past decade, many researchers have developed MIS SBDs using dissimilar substrates like GaN, GaAs, InP, and Si. In the current situation, p-Si is widely used due to its low work function which is advantageous in MIS SBDs for having more rectification behavior [16,17]. Among the

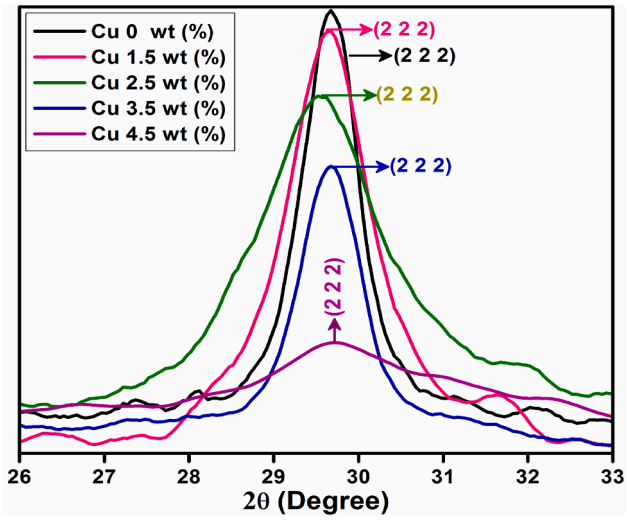


Fig.4. XRD peak position of undopedYb_2O_3 and Cu doped Yb_2O_3 films.

available techniques, the jet nebulizer spray pyrolysis (JNSP) process is used to cast nano structured thin films. Also, JNSP procedure possesses several advantages like high homogeneity, cost-effective and large area coating [18].

In this study, initially we prepared Copper doped Ytterbium oxide (Cu-Yb_2O_3) thin films on glass substrates with various Cu doping concentrations like 1.5, 2.5, 3.5 and 4.5 wt% at an optimized temperature of 550 °C and for the final device fabrication p-Si substrate was employed. The impact of Cu doping concentrations on optical and electrical characteristics of Cu doped Yb_2O_3 thin films were discussed. Then, the Al/Cu-Yb_2O_3/p-Si (MIS) Schottky diodes (SD) were casted using Cu-Yb_2O_3 thin films as an insulating layer between Al/p-Si interfaces. The diode

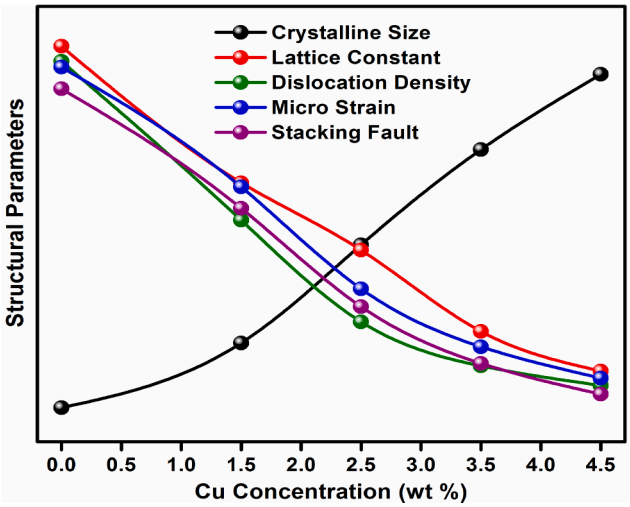


Fig.5. Structural parameters versus Cu concentration of different wt%.

parameters such as n, Φ_B and saturation current (I_o) of the fabricated diode were extracted by analyzing I-V characteristics for various doping concentration of Cu doped Yb_2O_3 thin films.

2. Experimental details

2.1. Chemical

In this present work, all the chemical reagents like rare earth materialytterbium (III) chloride hex hydrate ($YbCl_3{\cdot}6H_2O$) with (99.99% purity), and copper (II) chloride dehydrate ($CuCl_2{\cdot}2H_2O$) with (99.9% purity) were purchased from Sigma Aldrich, used without further process.

2.2. Preparationof Cu-Yb_2O_3 thinfilms

The economic JNSP route is used to grow a thin film of Cu-Yb_2O_3 on bare glass substrates cleaned thoroughly using hot Isopropyl alcohol (IPA) and acetone. For the preparation of undoped Yb_2O_3 thin films, 0.1 M of $YbCl_3{\cdot}6H_2O$ is dissolved in 10 ml of deionized water and is stirred for 45 min at 300 K using magnetic stirrer to get a homogeneous mixture. Similar procedure is adopted to prepare 0.1 mol of $CuCl_2{\cdot}2H_2O$ solution. The former solution is poured into the later $CuCl_2{\cdot}2H_2O$ solution with diverse concentrations of 1.5, 2.5, 3.5 and 4.5 wt% to prepare the precursor solutions. The prepared solutions (5 ml each) are then sprayed on the glass substrates maintained at an optimized temperature 550 °C using jet nebulizer spray pyrolysis technique. A substrate area of 2 × 2.5 cm^2 is used for preparing pure and Cu doped Yb_2O_3 films through effective JNSP method as presented in Fig. 1. This figure reveals the schematic diagram of the preparation mechanism of Cu-Yb_2O_3 thin films with different Cu doping concentrations.

2.3. Characterization techniques

At the outset, the quality of the prepared pure Yb_2O_3 and Cu-Yb_2O_3 thin films are analyzed through Rigaku Miniflex-II ($CuK\alpha_1$ radiation with λ = 1.5418 Å) with the diffraction range of (10–80°). A Stylus Profilometer detector (model: SJ-30) is used to measure the thickness of the film. Atomic force microscope (model: 5100 Pico LE) and Field emission scanning electron microscope (Zeiss Sigma model: FEI quanta 250) is used to analyze the surface and morphological behavior of Cu-Yb_2O_3 films. HRTEM image along with their SAED pattern images are observed using (TECHNAIT20) operated at 200 kV for fine surface morphological studies. The existence of elements like Yb, O and Cu has been ascertained by energy dispersive X-ray analysis (EDX). The optical property was studied using UV–vis Spectrometer (JASCO, model: V-770PC). Photoluminescence (PL) spectra are captured at 300 K through Spectrofluorometer (JASCO, model: FP-8300) in the wavelength range 200–750 nm. Finally, the electrical properties of the prepared thin films have been determined using two probe instruments at various temperatures (30–150 °C). Keithley electro-meter (Model: 6517B) is used to study the current Vs voltage (I–V) characteristics of the fabricated Al/Cu-Yb_2O_3/p-Si diode.

Table 1
Structural parameters of the prepared undoped and Cu doped Yb_2O_3 thin films.

Cu wt%	Thickness (nm)	Lattice constant (a) (nm)	Crystallite Size (D) (nm)	Dislocation Density δ × 10^{15} lines cm^{-4}	Stacking Fault SF × 10^{-2}	Micro Strain ε × 10^{-3}
0	156	1.047	11.959	6.992	0.6865	2.901
1.5	316	1.053	15.674	4.071	0.5216	2.213
2.5	448	1.044	21.309	2.203	0.3869	1.628
3.5	623	1.040	26.783	1.394	0.3179	1.295
4.5	841	1.038	31.105	1.034	0.2657	1.115

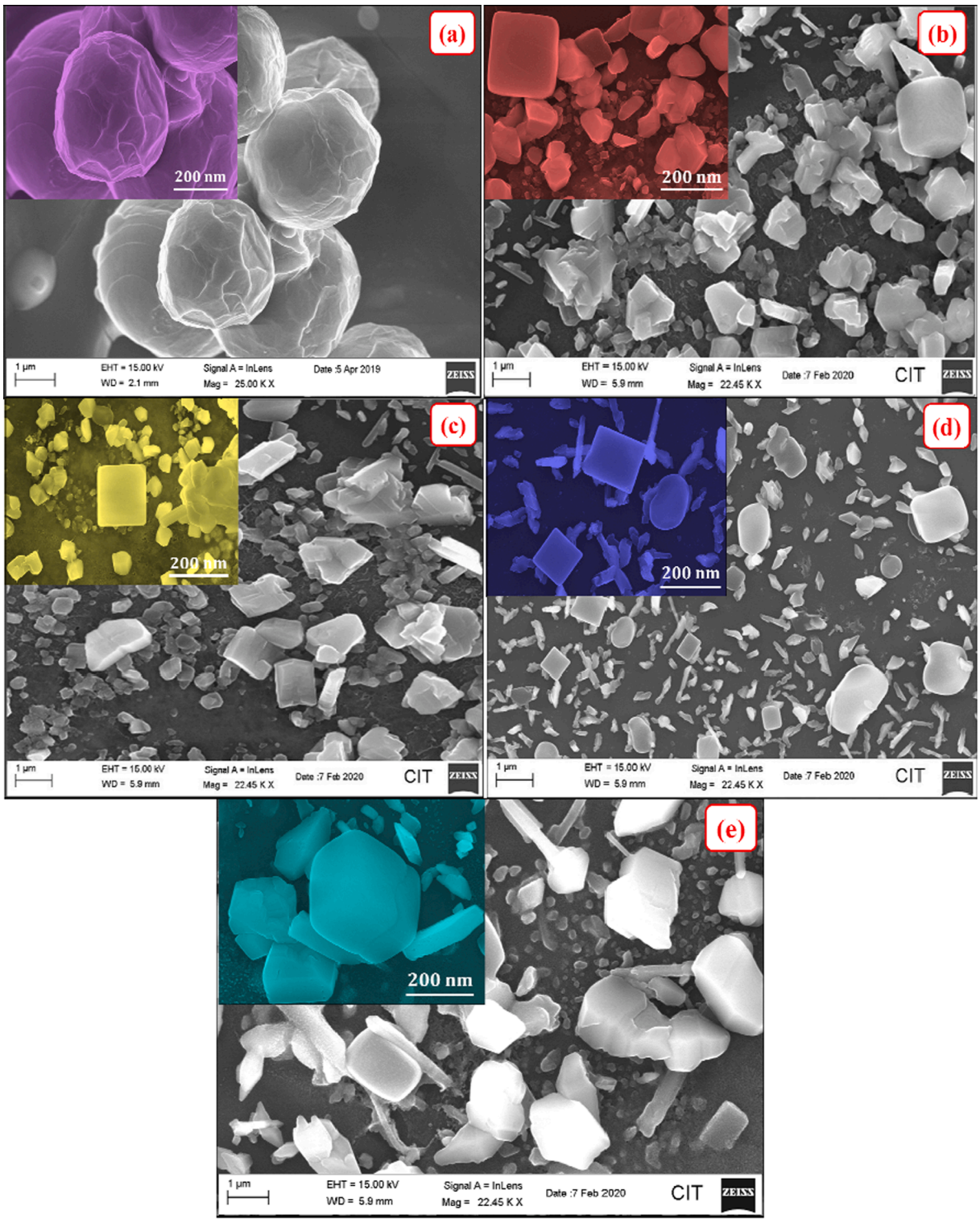


Fig. 6. FESEM images of the Cu-Yb_2O_3 films with different Cu doping concentrations (a) 0 wt% (b) 1.5 wt% (c) 2.5 wt% (d) 3.5 wt% (e) 4.5 wt%.

3. Results and discussion

3.1. Thickness variation of the Cu-Yb_2O_3 films

The thickness of Yb_2O_3 and Cu-Yb_2O_3 films with different Cu concentrations is revealed in Fig. 2. The thicknesses of the films are found to linearly rise with increasing Cu concentration. The measured film thicknesses are 156, 316, 448, 623, and 841 nm for 0, 1.5, 2.5, 3.5 and 4.5 wt% doped Cu-Yb_2O_3 thin films. Film thickness increases due to the strong bonding between the internal structures which could be possible by suitable doping. The higher film thicknesses have been observed in 4.5 wt% of Cu concentrations. Also, Cu concentration may lead to enhancement in the film thickness and lattice parameters. The deposition parameters such as substrate temperature, deposition time, mole ratio and carrier gas pressure determine the growth and quality of the film and hence the JNSP route has great influence on developing the thin

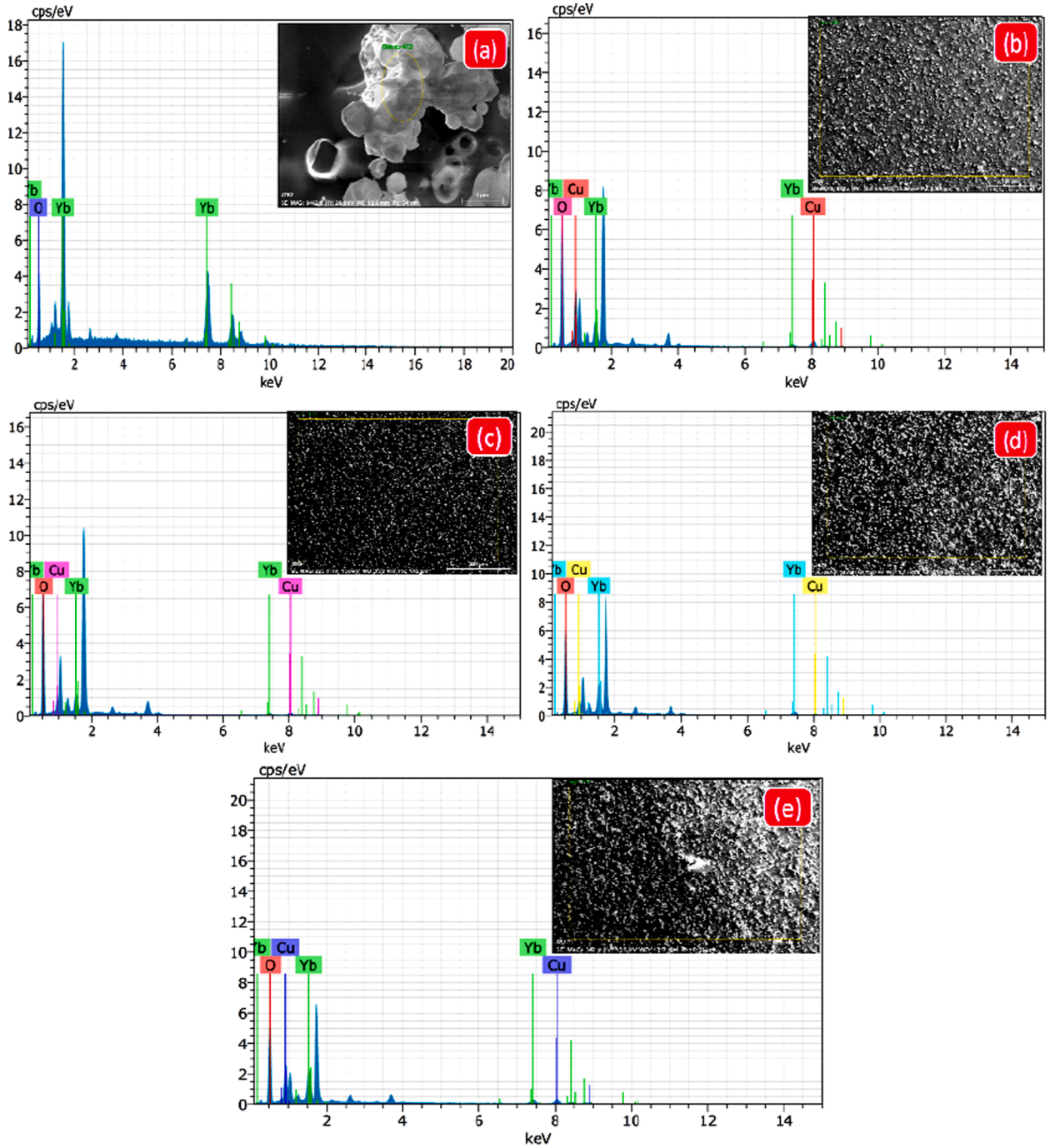


Fig. 7. Elemental analysis of the Cu-Yb_2O_3 films with different doping concentrations (a) 0 wt% (b) 1.5 wt% (c) 2.5 wt% (d) 3.5 wt% (e) 4.5 wt%.

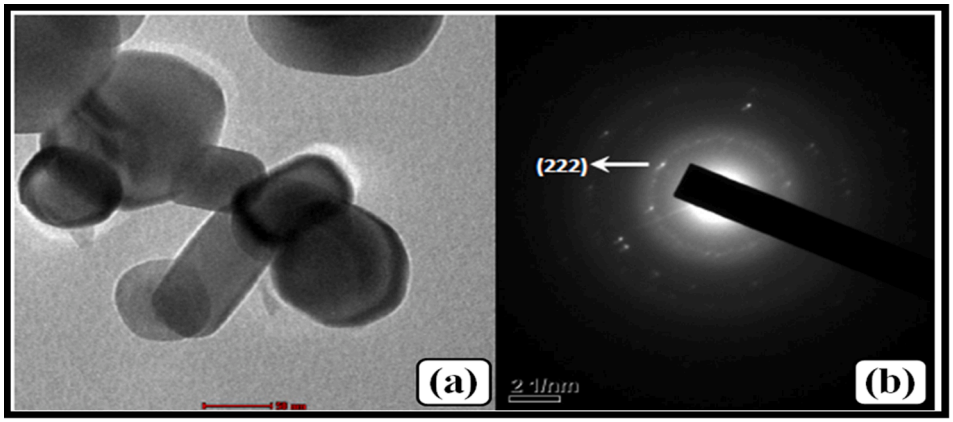


Fig. 8. (a-b) TEM image and SAED pattern of 4.5 wt% Cu doped Yb_2O_3 film.

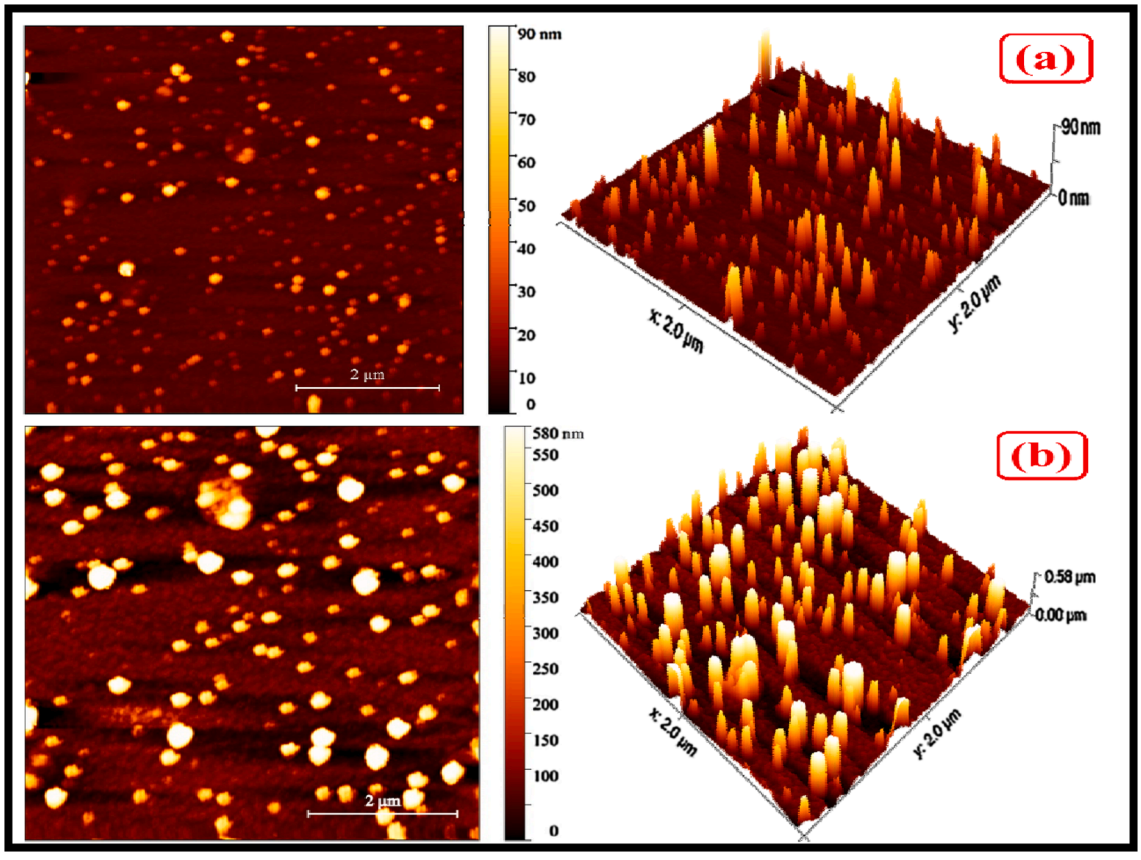


Fig.9. 2D and 3D AFM images of Cu doped Yb_2O_3 films (a) 1.5 wt% (b) 4.5 wt%.

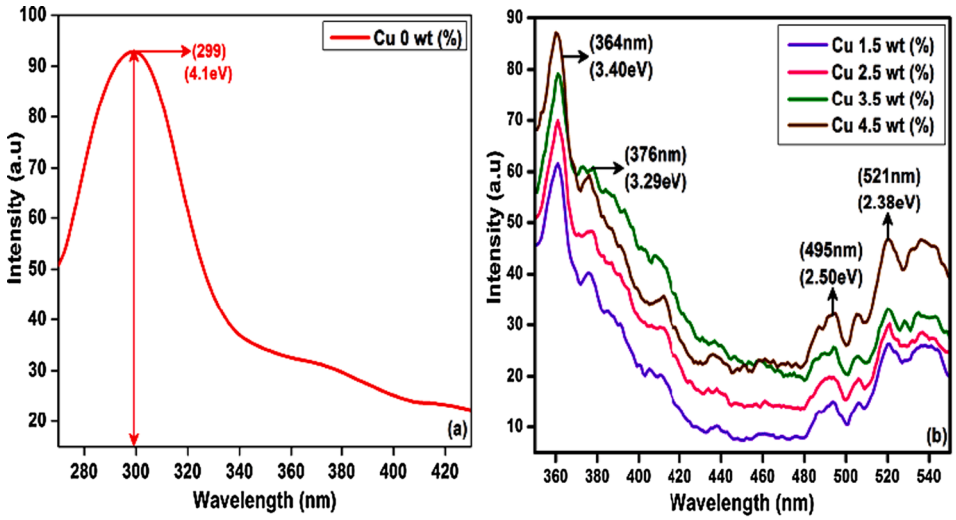


Fig. 10. PL spectrum of (a) undoped Yb_2O_3film (b) Cu doped Yb_2O_3 films.

layer films [19].

3.2. XRD analysis

Fig. 3 (a-e) indicates the XRD profiles of pure Yb_2O_3 film and Cu doped Yb_2O_3 films at different doping concentration. The XRD patterns of Yb_2O_3 correspond to main angle of diffraction peaks at 2θ values of 20.81°, 29.52°, 34.60°, 38.67°, 44.43°, 49.37° and 58.57° to their linked (h, k, l) planes of (2 1 1), (2 2 2), (4 0 0), (4 2 0), (1 3 4), (4 4 0) and (6 2 2), respectively. This result also shows the formation of polycrystalline nature with a cubic structure (JCPDS No. 65-5792). However, XRD patterns recorded showed the sharp peaks, indicating its crystalline structure. Some additional peaks were also observed along with Yb_2O_3 phase for higher Cu doping concentration of 3.5 and 4.5 wt% corresponding to CuO monoclinic structure (JCPDS No. 48-1548). These additional diffraction peaks at 35.49° and 35.56° are found to be reflected from (0 0 2) and $(11\bar{1})$ plane of crystallized CuO in the film. These peaks are very well matched for monoclinic phase [20]. They are appeared only at the increased Cu doping concentration. Moreover, the doping of Cu does not show much variation in the crystal structure of Yb_2O_3 thin films [21]. A minute peak shift towards lower angle corresponding to undoped Yb_2O_3 is observed which clearly indicates the successful incorporation of Cu^{2+} ions (0.73 Å) in the Yb^{3+} (0.86 Å) lattice which leads to an increase in the lattice values and phase changes of unit cell in Cu doped Yb_2O_3 thin films [22]. Fig. 4 clearly shows that the intensity of the predominant peaks decreases due to increase in the Cu doping concentration. The average crystalline size (D_{ave}) of undoped Yb_2O_3 film and Cu doped Yb_2O_3 films is determined using Scherrer equation given as follows [23].

$$Crystalline\ size(D_{avg}) = \frac{K\lambda}{\beta cos\theta} \quad (1)$$

where K represents Scherer's constant and β is the full width at half maximum intensity of the dominant peak.

The calculated average crystallite size of undoped Yb_2O_3 is 11.95 nm. Likewise, the D_{ave} of Cu-Yb_2O_3 is 15.67 nm for 1.5 wt% doping level, 21.30 nm for 2.5 wt%, 26.78 nm for 3.5 wt% and 31.10 nm for 4.5 wt%, respectively. This signifies that the D_{ave} increases on raising the Cu concentrations as shown in Fig. 5. The copper ion has a tiny radii, large ionic mobility, and low activation energy. So, it will be easier to transfer from trap to nucleation sites for these ions when growth of crystallites takes place, resulting in the growth of bigger crystallites because of low activation energy [24]. Also, the lattice constant (a), dislocation density (δ), micro strain (ε) and stacking fault (SF) are obtained by Eqs. (2)–(5) [23] and are summarized in the Table 1.

$$Band\ gap(a) = d \times \sqrt{h^2 + k^2 + l^2} \quad (2)$$

$$Dislocation\ density(\delta) = \frac{1}{D_{avg}^2} \quad (3)$$

$$Micro\ strain(\varepsilon) = \left[\left(\frac{\lambda}{D_{avg} sin\theta}\right) - \left(\frac{\beta}{tan\theta}\right)\right] \quad (4)$$

$$Stacking\ fault(SF) = \left[\left(\frac{2\pi^2}{45(3tan\theta)^{\frac{1}{2}}}\right) \times \beta\right] \quad (5)$$

where, D is the average crystallite size, λ is the wavelength (0.15418 nm) for CuKα, θ is the diffraction angle in degrees and d in Eq. (2) represents the inter planar distance. Fig. 5 shows that the lattice constant values (a) decreases with increase in Cu concentration. Furthermore, the values ε, δ and SF are noted to lessen as Cu concentration increases. These results clearly indicate that the key reason for rise in crystallite size is linked with lessening stacking fault and dislocation density [25–27]. The reduction of ε indicates the lessening of crystal imperfections and development of superior films [28–29]. XRD spectra reveal that the concentrations of Cu doping strongly influences the structural parameters of the prepared films.

3.3. Surface morphology and elemental composition analysis

Fig. 6 (a-e) shows the FESEM images of pure and Cu doped Yb_2O_3 films at an optimized substrate temperature of 550 °C. The surface morphology exhibits a continuous variation on doping with Cu into Yb_2O_3 film. The Cu concentration sturdily influences the surface morphology of Yb_2O_3 films. Fig. 6 (a) shows randomly oriented crack free and smooth surface of the fine tiny globular like structures having

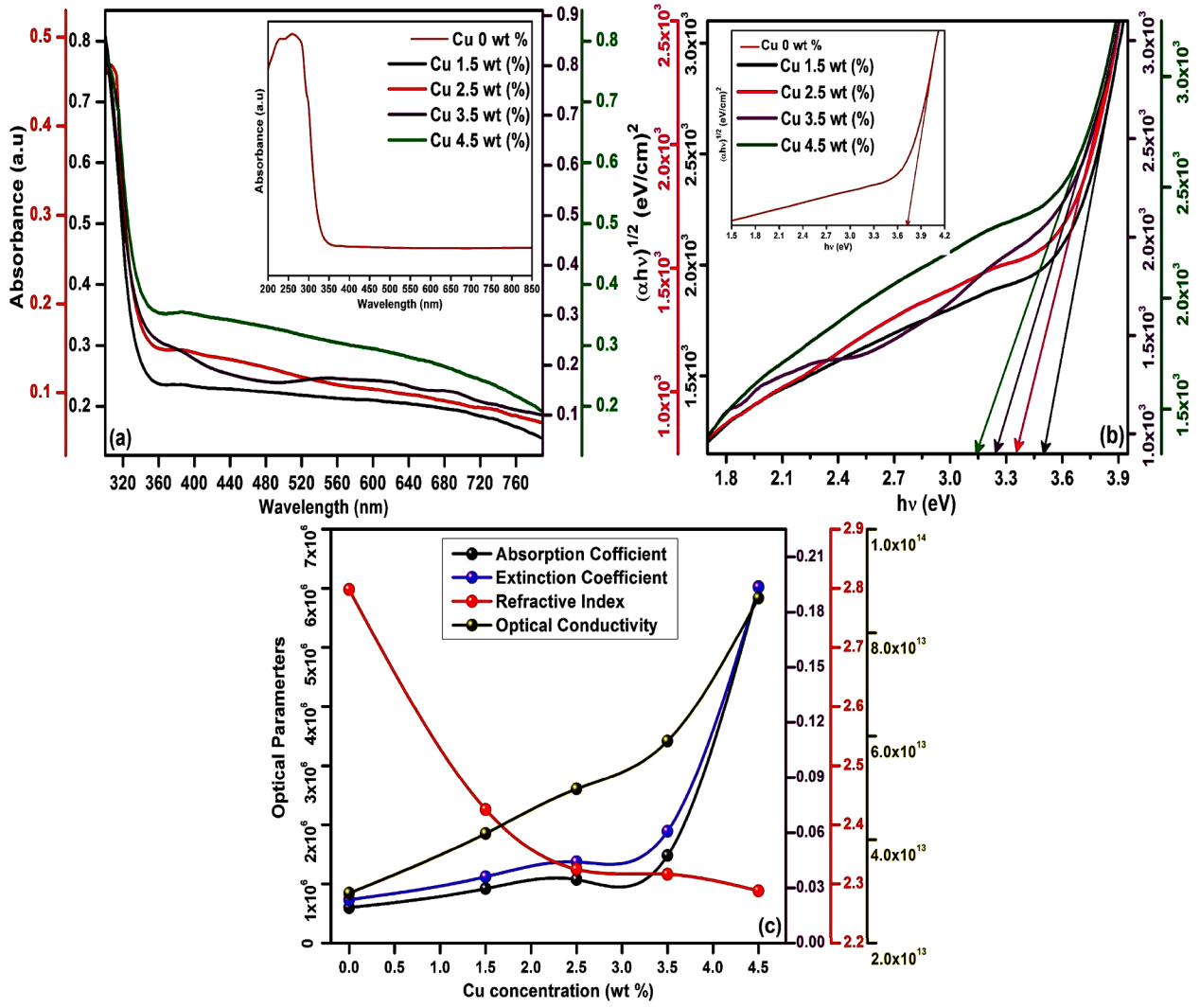


Fig. 11. (a) Absorbance Spectra, (b) plots of $(\alpha h\nu)^{1/2}$ Vs $h\nu$, (c) Average optical parameters for undoped Yb_2O_3 film and Cu doped Yb_2O_3 thin films obtained at different doping concentrations.

an average size of 11 nm for the pure Yb_2O_3 thin film. Fig. 6 (b–c) shows that the films with lower concentration like 1.5 and 2.5 wt % exhibit randomly arranged, crack free surface of sub micro sized granular like very fine cubic particles having a size between 15.67 and 21.30 nm. This result agrees well and good with the Yb_2O_3 phase. Interestingly, when the Cu concentration in the film was increased to 3.5 and 4.5 wt %, the particles changes to monoclinic phase to form a non-uniform sea coral like structure, with an average size between 26.78 and 31.10 nm as shown in Fig. 6 (d-e). In addition, particle size distributions (PSD) of Cu-Yb_2O_3 films are analyzed by using image J software. The particle size distribution of Cu-Yb_2O_3 thin films for different doping concentrations. The average value of the particle size is ~ 18.32. nm at undoped Yb_2O_3 thin films. Likewise, the particle sizes are ~27.25, 36.41, 47.79 and 59.33 nm for different doping concentrations of Cu and values are displayed in table 1. An increase in the Cu concentration leads to the formation of large particles on the surface as can be seen in Fig. 6 (d) and (e). The incorporation of Cu concentration highly affects the growth of granular like cubic phase owing to the effect of clustering and Cu atomic radius very small compared to the Yb atomic radius [30]. Moreover, the surface morphology and arrangement of grains supports the phase transformation in XRD from cubic to monoclinic structure in the Cu-Yb_2O_3 films at larger doping concentration is approved from FESEM

Table 2
Optical parameters of undoped and Cu doped Yb_2O_3 thin films.

Cu concentrations (wt %)	Absorption Coefficient (α) $(cm)^{-1}$	Extinction Coefficient (k)	Refractive Index (n)	Optical Conductivity (σ_{opt}) × 10^{13} (S/cm)	Band Gap (eV)
0	5.99×10^5	0.0236	2.798	2.96	3.68
1.5	9.18×10^5	0.0360	2.426	4.12	3.50
2.5	1.07×10^6	0.0440	2.325	4.98	3.36
3.5	1.48×10^6	0.0608	2.316	5.91	3.24
4.5	6.03×10^6	0.1935	2.288	8.67	3.14

Table 3
Electrical parameters of undoped and Cu doped Yb_2O_3 thin films.

Cu concentrations (wt%)	Resistivity (ρ) (Ω·cm)	Average conductivity (σ_{dc}) × 10^{-15} (S/cm)	Activation energy (E_a) (eV)
0	1.11×10^{15}	1.08	0.395
1.5	7.75×10^{14}	1.55	0.377
2.5	6.32×10^{14}	1.87	0.359
3.5	4.91×10^{14}	2.28	0.325
4.5	4.28×10^{14}	2.76	0.283

images. The modified morphology confirms the lessening of leakage current in the device and improvement in the electrical conductivity (σ) owing to the higher surface to volume ratios. In addition, EDX spectra of spray deposited Yb_2O_3 films of different Cu doping concentrations such as 1.5, 2.5, 3.5, and 4.5 wt% is demonstrated in Fig. 7 (a-e). Fig. 7(a-e), authorize the Yb, Cu, and O peaks close to stoichiometric ratio in Cu doped Yb_2O_3 thin films. The atomic % of Copper concentrations increases from 6.44, 7.26, 8.10, and 8.49 Cu-Yb_2O_3 films coated with different doping concentrations. The additional peaks in the EDS spectra are related to glass substrate (Si, O, Mg. Na, Ca, Al) and Au used for sample coating [31]. Particularly, ytterbium content is found to fall with the rise in oxygen content due to the increasing Cu doping concentrations. No peaks were observed related to elements other than copper (Cu), Yb, and O in the EDX spectra. From the EDX results, the Cu-Yb_2O_3 thin films indicate the strongly influence of Cu in the Yb lattice at higher doping concentration. This result reveals that Cu plays a key role in the MIS SDs and enhances the device performance [32].

3.4. Transmission electron microscopic analysis

The crystal system of casted films was examined with selected area electron diffraction (SAED) of TEM. Fig. 8 (a-b) show TEM micrographs with the SAED pattern of the prepared Cu-Yb_2O_3 film having 4.5 wt%. Fig. 8(a) shows the presence of tiny spherical particles with mean size of NPs in between 11 and 53 nm. The microscopic image shows the variation of the average size of nano particles in between such a small range can be considered roughly as the nearly uniform distribution and it is clearly observed to have some agglomeration [33]. The SAED pattern in Fig. 8 (b) reveals bright spots, which indicates the polycrystalline nature [34].

3.5. Atomic force microscopic analysis

Fig. 9 (a-b) show the 2D and 3D AFM topography images of Cu-Yb_2O_3 thin films deposited at 550 °C for lower and higher doping concentration like 1.5 and 4.5 wt%. Fig. 9 (a) exhibits evenly distributed conical columnar micro structure with measured average roughness (R_a) 17.45 and area root mean square (RMS) of 28.87 nm. When the doping concentration was increased to 4.5 wt%, the measured average roughness (R_a) is 69.66 and area root mean square (RMS) value is 124.34 nm respectively. It is clear that the increase in doping concentrations strongly influences the surface morphology of the deposited films as shown in Fig. 9(b). The AFM images reveal the increase in the surface roughness with the doping concentration. The film thickness also increases with increasing in doping concentration favoring the enhancement in the optical property of the films. Thus, the morphological disparities are in good pact with FESEM images [35].

3.6. PL analysis

Fig. 10 (a)-(b) represent PL spectra of pure and doped Yb_2O_3 films with different concentration like 1.5–4.5 wt% of Cu deposited at 550 °C optimized substrate temperature. The undoped Yb_2O_3 film indicates a PL peak in the broad UV emission peak centered at 299 nm (4.1 eV) as shown in Fig. 10(a). Fig. 10(b) shows the existence of four PL peaks in the emission band. When the doping concentration increases, the film exhibits a sharp UV-NBE peak at 364 nm (3.40 eV) and another emission peak at 376 nm (3.29 eV), a blue emission peak around 495 nm (2.50 eV) and a sharp visible green emission peak 521 nm (2.38 eV). It clearly indicates the shifting of peak position to higher energy side. When the Cu doping concentration increases in Yb_2O_3 films, the PL nature of the film has a handy connection with crystallinity due to the decrement in the density of defect in the film with enhancement of crystallinity as well as on the crystallite size [36–37]. The UV emission peak corresponds to emission attributed to the oxygen vacancies and green emission peak due to the presence of interstitial V_O and D_I with high doping concentrations. These results support the enhancement in the optical behavior and it helps to improve the device performance which is preferable for the MIS SDs. Moreover, the photo luminescence results reveal the existence of strong and sharp emission bands for the prepared films at 4.5 wt % compared with other deposited films [38]. Hence, the results correlate well with the surface morphology and structural changes with the increase in Cu concentration as observed in FESEM and XRD results.

3.7. UV–Visible spectroscopy analysis

Fig. 11 (a) reveals that the absorption spectra of undoped Yb_2O_3 film and Cu doped Yb_2O_3 films with different concentrations like 1.5, 2.5, 3.5, and 4.5 wt % deposited at 550 °C. From the Fig. 11 (a), a strong optical absorption peak is observed below 350 nm. It is clearly visible that the rise in Cu concentration causes the value of absorption to shift slightly to bigger wavelength region in contrast to the undoped Yb_2O_3, because of the deep bluish pigmentation of films, roughness of surface and increase in the grain boundaries and also due to the charge carriers induced by Cu doping [39–40]. The maximum absorbance is observed for 4.5 wt% of Cu-Yb_2O_3thin films. From the UV–Vis spectra, the optical energy-gap (Eg) values are obtained from the following Eq. (6) [41].

$$Band\ gap(\alpha h\nu) = A(h\nu - E)^n \quad (6)$$

The optical band gap values were determined from Tauc's plot, among $(\alpha h\nu)^{1/2}$ vs. $(h\nu)$ for Cu-Yb_2O_3 films as shown in Fig. 11 (b). When n is 2, it specifies indirectly permitted transitions and intercept on E-axis gives the values of E_g. The energy gap values of 3.68, 3.50, 3.36, 3.24, and 3.14 eV respectively for pure Yb_2O_3 film and Cu doped Yb_2O_3 films are observed from the extrapolation of the vertical straight line to E-axis. However, we have also calculated the direct band gap of the films and found in a range of 4.6 to 5.0 eV [42]. The band gap of undoped Yb_2O_3 film was found to be higher than doped Yb_2O_3 films because of increases in Fermi energy level and DOS of E shrinking and another possible reaction is V_O that will generate effects near to Fermi level which moves towards CB [43]. From these results, E shrinks with Cu concentrations and these outputs are in good agreement with semiconducting nature of casted Cu-Yb_2O_3 films, which is more appropriate for the MIS SD. The absorption co-efficient (α), refractive index (n), extinction co-efficient (k), and optical conductivity (σ_{opt}) can be calculated by using the following relations (7–10) [41].

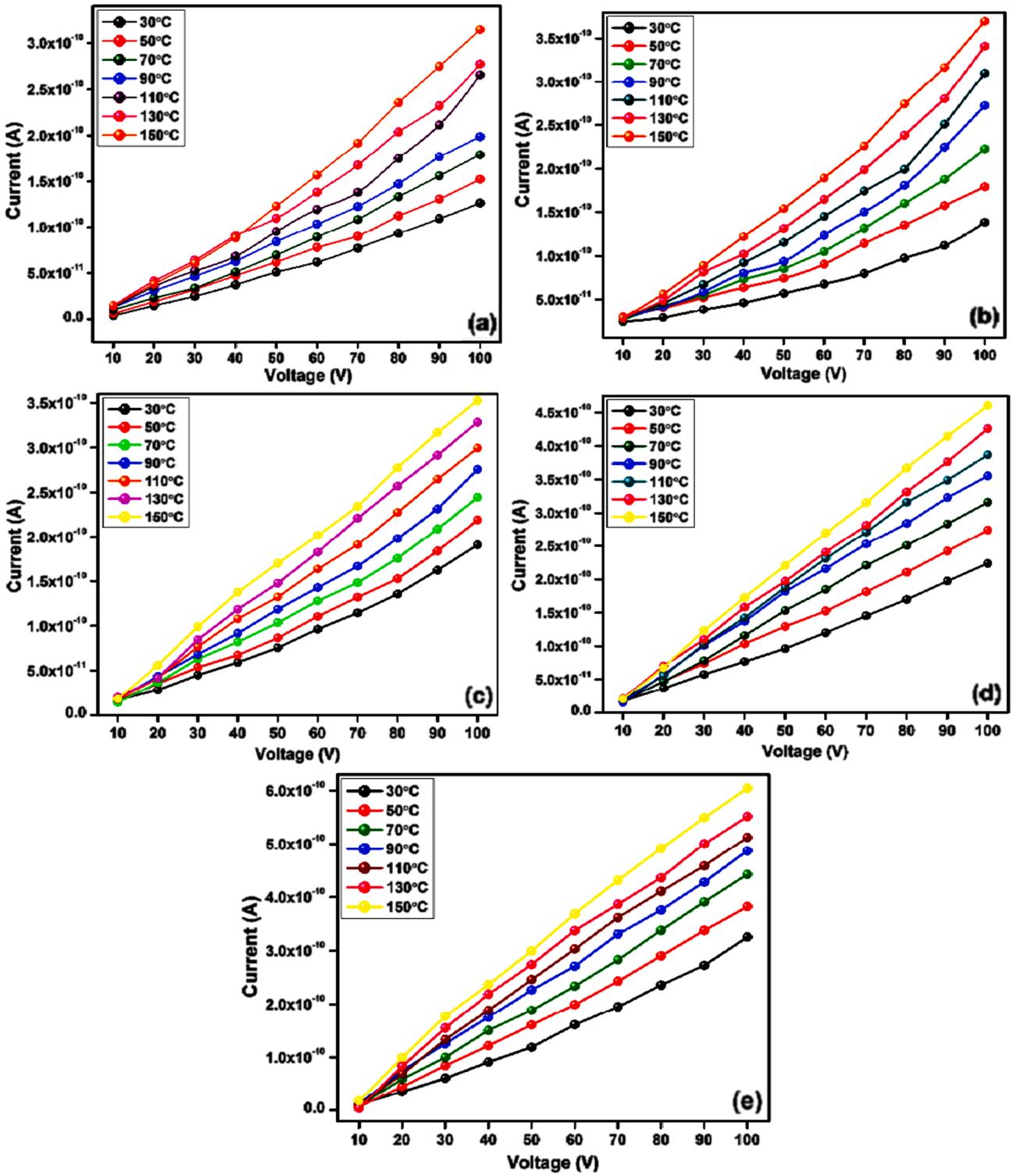


Fig. 12. Current –Voltage (I-V) plots of the prepared films at different temperature (a) undoped Yb_2O_3 and (b-e) 1.5, 2.5, 3.5, and 4.5 wt%.

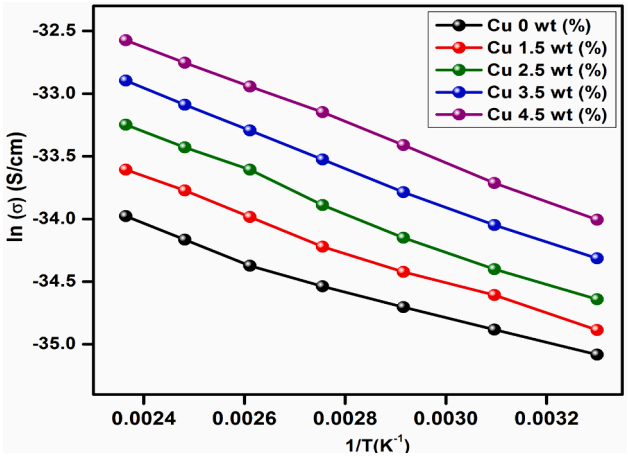


Fig.13. Arrhenius plots of ln (σ) vs 1/T of Cu-Yb_2O_3 films for different Cu wt%.

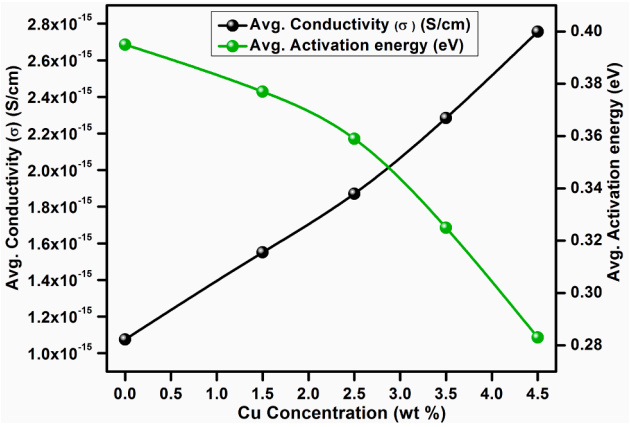


Fig.14. Average conductivity and activation energy versus Cu concentrations (wt %).

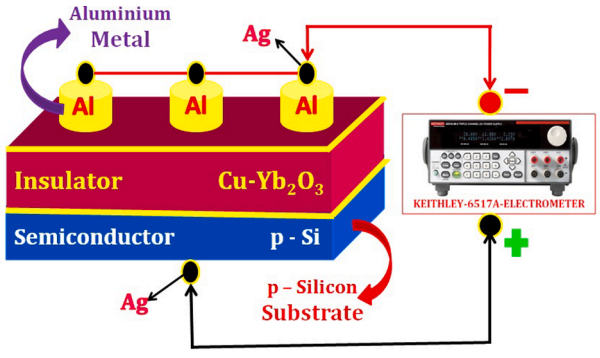


Fig. 15. Schematic diagram of Al/Cu-Yb_2O_3/p-Si (MIS) Schottkydiode.

$$Absorption\ Co-efficient(\alpha) = \left[\frac{1}{t}\right] ln \left[\frac{1}{T}\right] \quad (7)$$

$$Refractive\ index(n) = \left[\frac{1+R}{1-R}\right] + \left[\sqrt{\frac{4R}{(1-R)^2 - k^2}}\right] \quad (8)$$

$$Extinction\ Co-efficient(k) = \left[\frac{\alpha\lambda}{4\pi}\right] \quad (9)$$

$$Optical\ Conductivity(\sigma_{opt}) = \left[\frac{nc\alpha}{4\pi}\right] \quad (10)$$

The changes of α, k, n and σ_{opt} values with different Cu concentrations are shown in Fig. 11 (c) and values are summarized in Table 2. The refractive index (n) of the film gradually decreases from 2.798 to 2.288 which are due to the increase in the Cu concentration, variation of packing density and higher film thickness. The value of α, k and σ_{opt} parameters of the Cu-Yb_2O_3 film are noticed to be greater at higher content of Cu wt. % in Yb_2O_3 films [44]. These results influence the electronic transitions among VB and CB, which shrinks the E values of Cu-Yb_2O_3 films. Moreover, Cu sturdily affects the optical constants of Yb_2O_3 films, which could have an impact of the SDs.

3.8. DC electrical conductivity

The dc conductivity (σ_{dc}) of undoped Yb_2O_3 film and Cu-Yb_2O_3 films at different Cu concentrations (1.5, 2.5, 3.5 & 4.5 wt%) are measured by two probe setup with applying voltages from 10 to 100 V (step of 10 V) along with the variation temperature from 30 to 150 °C. The obtained resistivity (ρ) values of all the films are given in Table 3. It is observed that the value of ρ decreases on increasing the Cu concentrations in the Yb_2O_3 thin films. This case would considerably decrease the ρ of the film and gets a better mobility of the charge carriers [45].

$$Electrical\ conductivity(\sigma_{dc}) = \frac{t}{RA}\frac{s}{cm} \quad (11)$$

Here R, t and A represents resistance, thickness and area of the film. When Cu concentrations increase from 1.5 to 4.5 wt%, the electrical conductivity of Cu-Yb_2O_3 films improves linearly as shown in Fig. 12(a-e). The highest electrical conductivity (σ_{dc}) is obtained for a doping concentration of 4.5 wt%. As seen in Table 3, the mean conductivity varies from 1.08 × 10^{-15} to 2.76 × 10^{-15} S/cm. This clearly indicates that the films are of insulating nature which supports SDs. Besides, the highest average conductivity is obtained for Cu doping concentration with 4.5 wt% as shown in Fig. 12 (e), which is attributed to the presence of oxygen vacancies and create extra free electrons in VB and so shrinking the band gap between Fermi level and CB [46]. Moreover, these case results from the electrons around atoms of semiconductors that breaks away from their covalent bond and move freely on the lattice site. The activation energy (E_a) was determined from Arrhenius plot by:

$$Activation\ energy(\sigma_{dc}) = \sigma_o exp\left[\frac{-E_a}{K_B T}\right] \quad (12)$$

The values of E_a fluctuate from 0.395 to 0.284 eV with an increase of doping concentration. Fig. 13 reveals the Arrhenius plot of ln (σ) vs 1/T. It is found that the E_a value of undoped Yb_2O_3 thin film is 0.395 eV. With further increase in doping concentration, the E_a value reduces to 0.284 eV. This result clearly indicates the successful incorporation of Cu ions in the Yb ions lattice [47]. Furthermore, the changes in activation energy are due to the surface structure, crystalline phase, lattice dislocations and imperfections of higher doping concentrations of films [48]. The obtained mean conductivity improves where as the linked mean resistivity and E_a lessens. These results suggest that the increased electrical conductivity helps to improve the device performance and impacts the performance SDs. Fig. 14 clearly shows electrical constants vs Cu doping concentrations.

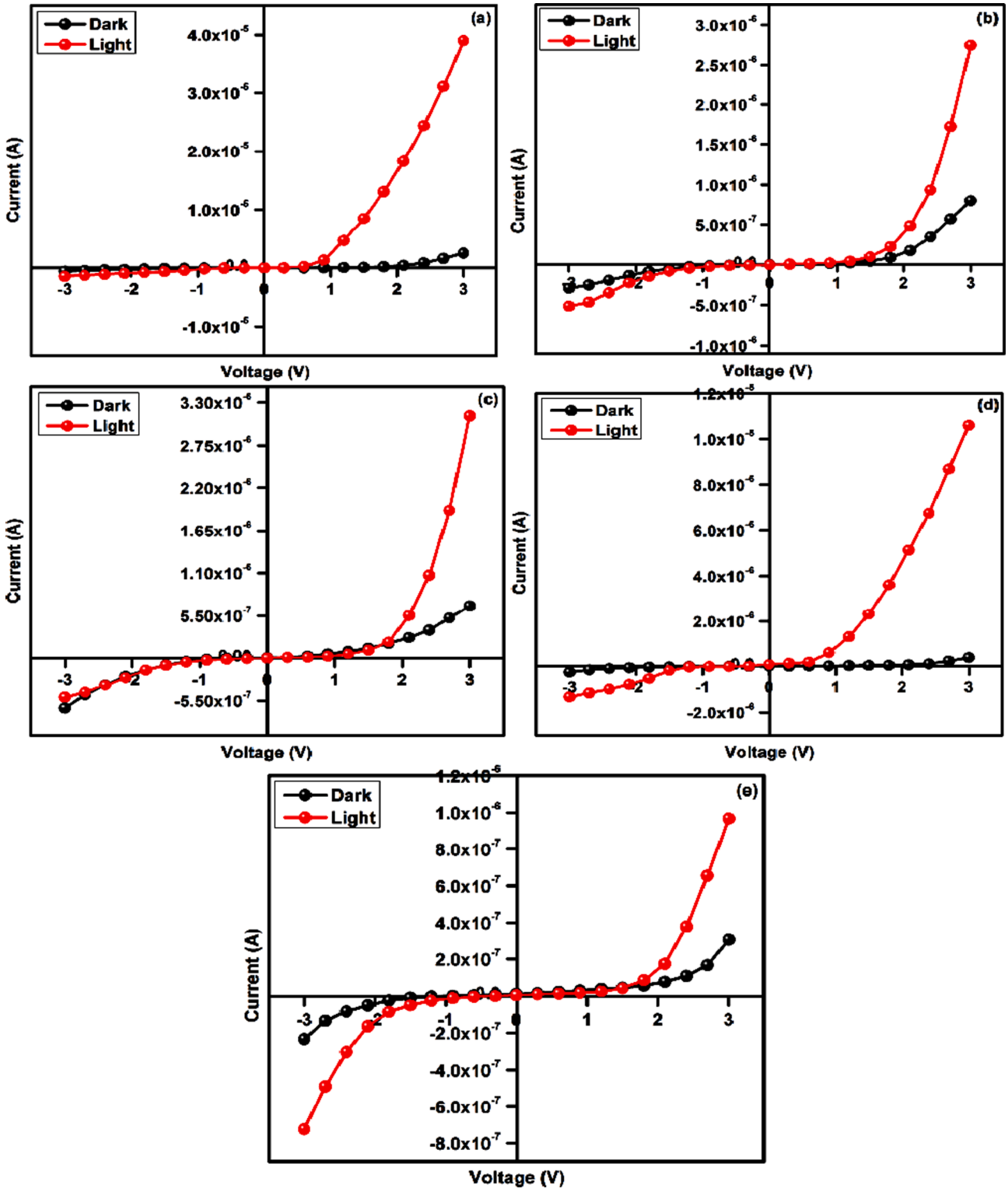


Fig. 16. I-V plots of Al/Cu-Yb_2O_3/p-Si Schottky barrier diodes with different doping concentrations (a) 0 wt% (b) 1.5 wt% (c) 2.5 wt% (d) 3.5 wt% (e) 4.5 wt%.

Table 4
Electrical parameters of Al/Cu-Yb_2O_3/p-Si (MIS) Schottky Diodes with different Cu doping concentrations.

Cu Concentrations (wt%)	Ideality factor (n)		Barrier height Φ_B (eV)		Saturation current (I_o) (A)	
	Dark	Light	Dark	Light	Dark	Light
0	2.537	2.059	0.789	0.638	4.65×10^{-07}	8.75×10^{-04}
1.5	2.262	1.889	0.847	0.657	2.83×10^{-07}	5.03×10^{-04}
2.5	2.206	1.845	0.868	0.675	1.26×10^{-07}	2.02×10^{-04}
3.5	2.154	1.797	0.892	0.723	5.12×10^{-08}	8.30×10^{-05}
4.5	2.120	1.757	0.911	0.754	2.45×10^{-08}	5.82×10^{-05}

4. Fabrication of Al/Cu-Yb_2O_3/p-Si Schottky diodes

The Al/Cu-Yb_2O_3/p-Si (MIS) SDs is casted on p-type Si wafer. Prior to depositing the diode, the wafer was cleaned well and immersed in the mixture of $H_2SO_4 + H_2O_2$ taken in the ratio of 3:1. These aids to evade undesirable oxide layer on the Si wafer. The layer of Cu-Yb_2O_3 was deposited by JNSP technique. Aluminum (Al) metal contactis used on the Cu-Yb_2O_3/p-Si structure via dc magnetron sputtering with the standard pressure of 6 mbar. The fabricated MIS diodes were dried in air for 12 hrs inside a clean chamber. The Ag paste was employed on either side of MIS diode for better electrical conductivity, low sheet resistance and is dried at room temperature for 5–6 hrs. The structure of the prepared MIS diode is publicized in Fig. 15.

4.1. I-V characteristics of Al/Cu-Yb_2O_3/p-Si Schottky barrier diode

From the Fig. 16 (a-e) show the I-V nature of fabricated MIS diode. The ohmic behavior of MIS diode is analyzed for different doping concentrations viz. 1.5, 2.5, 3.5, and 4.5 wt% of Cu. The parameters of MIS diode are studied under dark and light conditions. Fig. 16 illustrates the graphics of both reverse and forward current of MIS SDs measured by applying bias voltages −3 to + 3 V (in stet of 0.3 V). The current density (J = I/A) of SD for V⩾3 K_BT/q was determined by thermionic emission (TE) theory and given by the following equations [49].

$$Current\ Density(J) = J_o exp\left[\left(\frac{qV}{nK_BT}\right) - 1\right] \quad (13)$$

$$ReverseSaturationCurrent I_0 = J_0 A = AA^* T^2 exp(-\frac{q\phi_B}{K_B T}) J_o = A^* T^2 exp\left(-\frac{q\phi_B}{K_B T}\right) \quad (14)$$

Here Φ_B can be evaluated using Eq. (14) and A* stands for Richardson constant (=32 A/cm^2.K^2 for p-Si). Besides, the I_0 value can be derived from intercept of linear portion of forward-bias ln (I-V) curve. As seen in the I-V curves of Fig. 16, each MIS diode indicates positive response on testing of device below light. These outcomes reveal that prepared diodes possess photo conducting nature [50–51]. The attained I_o values in dark condition varies from $4.65 \times 10^{-7}$to 2.45×10^{-8} A, which is found to be improved in light condition from 8.75×10^{-4} to 5.82×10^{-5} A as given in Table 4. The obtained results suggest that, the device performance and σ values of the Al/Cu-Yb_2O_3/p-Si diodes are improving due to the successfully incorporation of Cu ions [52–53]. The other parameters such as ideality factor (n) & barrier height (Φ_B) are extracted from Eqs. (15) & (16), respectively [49].

$$Ideality\ Factor(n) = \left[\frac{q}{K_BT}\left(\frac{dV}{d(InJ)}\right)\right] \quad (15)$$

$$Barrier\ Height(\Phi_B) = \left[\frac{K_BT}{q} ln\left(\frac{AA^*T^2}{I_0}\right)\right] \quad (16)$$

Fig. 17 (a-e) clearly shows that the ln J-V plots of Al/Cu-Yb_2O_3/p-Si (MIS) SDs with different Cu doping concentrations. The n values are derived through linear portion of the forward-bias ln(J)-V curve. The obtained n and Φ_B quantities are presented in Table 4. It is clear that for an increase in the Cu doping concentration, the n values are found to be decreased from 2.537 to 2.12 under dark conditions. Fascinatingly, the MIS diodes studied below illumination condition indicates the lesser n values of 2.059 to 1.757 compared to dark condition. An experimental data designates that the diode has n value i.e. ˃1. It is because of the drop in the potential in the interface layers and existence of extra current and recombining of current via interface states amongst the semiconductors, insulator layers [54–55]. This may be attributed to the generation of electron-hole pair that may rise after light absorption. Furthermore, the higher ideality factor values of the diode might be ascribed to the existence of thin interfacial native (SiO_2) layer among the metal (Al) semiconductor (Si) interfaces. The Al/Cu-Yb_2O_3/p-Si (MIS) diodes under light give a huge number of charge carriers generated by light that raises the current. However, in dark, the current is reduced because of the reduction in the charge carriers and the other reason being specific distribution of interface state, potential drop at interfacial layer, image force effect, and the tunneling current through the interfacial layer [56–58]. Additionally, the barrier height (Φ_B) is found to be increased gently under dark and light condition with higher doping concentration of Cu-Yb_2O_3 [59–60]. The barrier height (Φ_B) observed in dark condition changes from 0.789 to 0.911 eV and under light condition from 0.638 to 0.754 eV. As a result, the maximum Φ_B and minimum n value are obtained for MIS diode having Cu doping concentration of 4.5 wt% in both dark and light condition.

5. Conclusion

We have successfully fabricated the Al/Cu-Yb_2O_3/p-Si (MIS) SDs using Cu-Yb_2O_3 films having various Cu doping concentrations as an insulating layer. The XRD pattern reveals the poly crystalline nature of cubic system of casted Cu-Yb_2O_3 thin films and the mean crystallite size of 31 nm is noticed for Cu-Yb_2O_3 films casted with 4.5 wt% of Cu. The structure of Cu-Yb_2O_3 films was recorded through FESEM. The extreme absorption and smallest energy gap of (3.14 eV) was noticed for 4.5 wt% of Cu-Yb_2O_3 films. The EDX profile showed the presence of Cu in Yb_2O_3 films. The AFM analysis revealed a higher roughness and RMS value at larger doping concentration of 4.5 wt% of Cu. The photoluminescence spectrum of Cu-Yb_2O_3 thin films indicates a strong and broad emission bands at 364 nm (3.40 eV). DC electrical study reveals a maximum conductivity and minimum activation energy for larger doping concentration. From MIS SDs, the experimental result shows an improved Φ_B and decreased n values for higher doping concentrations. From the diode results, the higher doping concentrations of 4.5 wt% exhibits better performance SDs when compared to undoped Yb_2O_3 thin film. The barrier height (Φ_B) observed in dark condition varies between 0.789 eV and 0.911 eV and under light condition from 0.638 eV to 0.754 eV for Cu-Yb_2O_3 thin films. The obtained results confirm that the fabricated Al/Cu-Y_b2O_3/p-Si (MIS) Schottky diodes are highly suitable for the advanced optoelectronic, microelectronic, and high-speed switching device applications.

Declaration of Competing Interest

The authors declare that they have no known competing financial interests or personal relationships that could have appeared to influence the work reported in this paper.

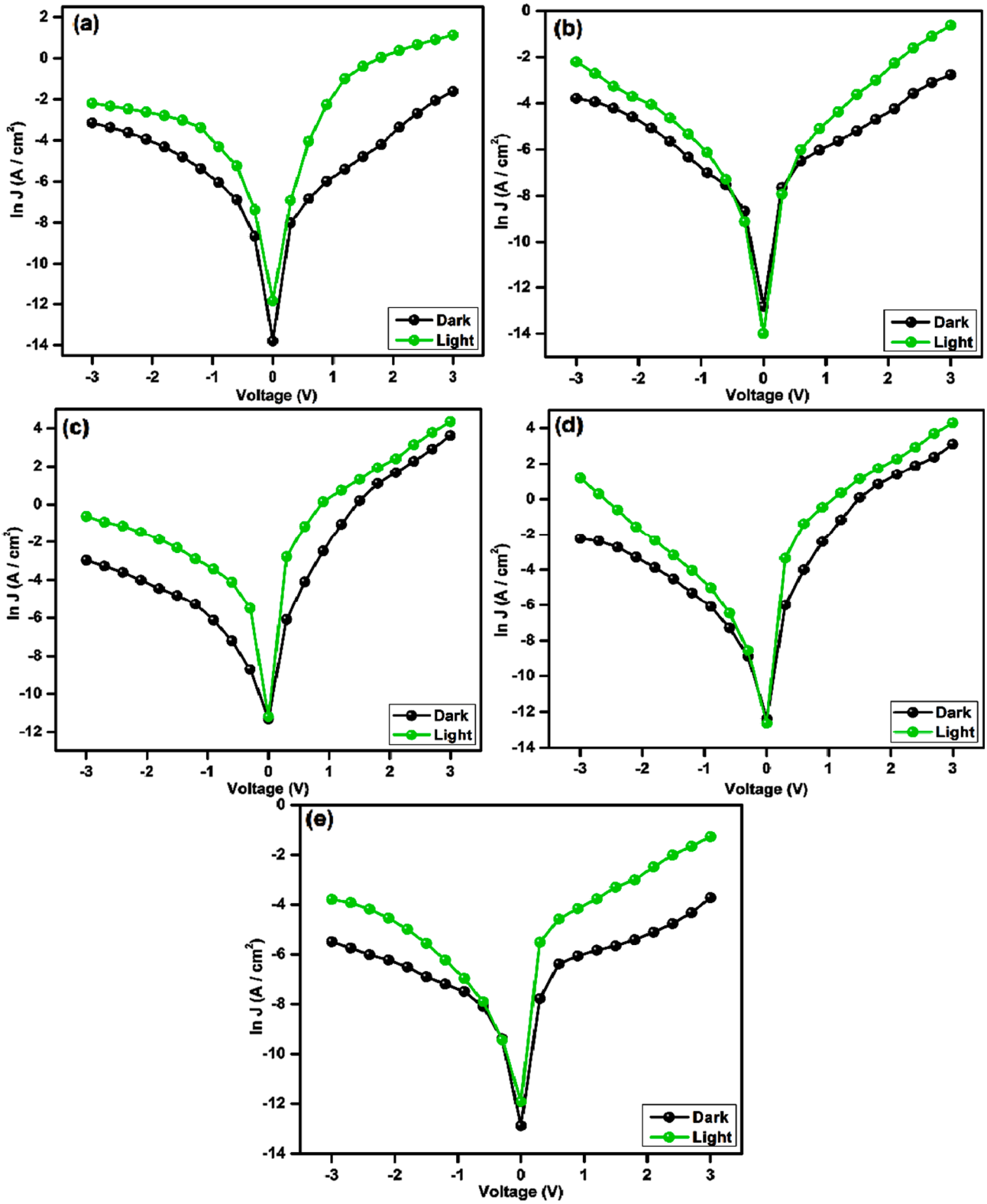


Fig. 17. ln J-Vplots of Al/Cu-Yb_2O_3/p-Si Schottky barrier diodes with different doping concentrations (a) 0 wt% (b) 1.5 wt% (c) 2.5 wt% (d) 3.5 wt% (e) 4.5 wt%.

Acknowledgement

The authors would like to express their gratitude to Advance Research Instrumentation Centre (ARIC), Sri Ramakrishna Mission Vidyalaya College of Arts and Science, Coimbatore for providing instrument facilities. Author M. Shkir would like to express his gratitude to the Deanship of Scientific Research at King Khalid University, Abha, Saudi Arabia for funding this work through Research Groups Program under Grant No. R. G.P.2/60/42.

References

[1] Hazem K. Khanfar, Atef F. Qasrawi, Yasmeen A. Zakarneh, N.M. Gasanly, Design and applications of Yb/Ga2Se3/C schottky barriers, IEEE Sens. J. 17 (14) (2017), https://doi.org/10.1109/JSEN.2017.2702710.

[2] V. Rajagopal Reddy, L. Dasaradha Rao, V. Janardhanam, Min-Sung Kang and Chel-Jong Choi, Electrical properties and interface states of rare-earth metal ytterbium schottky contacts to p-type InP, Mater. Trans. 54 (12) (2013) 2173–2179, https://doi.org/10.2320/matertrans.M2013281.

[3] M.S. Henriques, A.C. Ferreira, A. Cruz, L.M. Ferreira, J.B. Branco, P. Brázda, K. Jurek, T. Stora, A.P. Gonçalves, Preparation of Yb_2O_3 submicron- and nano-materials via electrospinning, Ceram. Int. 41 (2015) 10795–10802, https://doi.org/10.1016/j.ceramint.2015.05.017.

[4] T.-M. Pan, C.-H. Chen, F.-H. Chen, Y.-S. Huang, J.-L. Her, Structural and electrical characteristics of Yb_2O_3 and $YbTi_xO_y$ gate dielectrics for α InGaZnO thin-film transistors, J. Display Technol. 1551–319X (2013), https://doi.org/10.1109/JDT.2014.2380453.

[5] M. Balaji, J. Chandrasekaran, M. Raja, R. Marnadu, M. Ramamurthy, Mohd, Shkir Fabrication of ON/OFF switching response based on n-Ni-doped MoO_3/ p-Si junction diodes using Ni-MoO_3 thin films as n-type layer prepared by JNS pyrolysis technique, Appl. Phys. A 126 (216) (2020), https://doi.org/10.1007/s00339-020-3392-0.

[6] Y. Munikrishna Reddy, T. Lakshmi Narasappa, R. Padman Suvarna, V. Rajagopal Reddy, Analysis of electrical properties and carrier transport mechanisms of Ru/Ti/n-InP Schottky diodes at room temperature, Int. J. New Technol. Sci. Eng. 2 (2) (2015) 2349–2780.

[7] Aysegul Kahraman, Huseyin Karacali, Ercan Yilmaz, Impact and origin of the oxide-interface traps in Al/Yb_2O_3/n-Si/Al on the electrical characteristics, J. Alloys Compd. 825 (2020) 154171, https://doi.org/10.1016/j.jallcom.2020.154171.

[8] A. Prnová, K. Bodišová, R. Klement, M. Migát, P. Veteška, M. Škrátek, I. Van Els Bruneel, D. Galusek Driessche, Preparation and characterization of Yb_2O_3–Al_2O_3 glasses by the Pechini sol–gel method combined with flame synthesis, Ceram. Int. 40 (2014) 6179–6184, https://doi.org/10.1016/j.ceramint.2013.11.071.

[9] S. Zargouni, S. El Whibi, E. Tessarolo, M. Rigon, A. Martucci, H. Ezzaouia, Structural properties and defect related luminescence of Yb-doped NiO sol-gel thin films, Superlattices Microstruct. 138 (2020) 106361, https://doi.org/10.1016/j.spmi.2019.106361.

[10] Nidhi Puri, Aman Rohilla, S.K. Chamoli, Ajit K. Mahapatro, Effect of ytterbium oxide deposition on micro structural and electrical properties of thin tantalum foil, Mater. Lett. 253 (2019) 67–70, https://doi.org/10.1016/j.matlet.2019.06.016.

[11] V. Rajagopal Reddy, D. Sri Silpa, V. Janardhanam, Hyung-Joong Yun, Rapid thermal annealing effects on the electrical, structural and morphological properties of Yb/ p-type InP Schottky Structure, Elecrron. Matter. Lett. 11 (1) (2015) 73–81, https://doi.org/10.1007/s13391-014-1368-y.

[12] M. Balaji, J. Chandrasekaran, M. Raja, Role of substrate temperatureon MoO_3 thin films by the JNS pyrolysis technique for P-N junction diode application, Mater. Sci. Semicond. Process. 43 (2016) 104–113, https://doi.org/10.1016/j.mssp.2015.12.009.

[13] A. BuyukbasUlusan, İ. Taşçıoğlu, A. Tataroğlu, F. Yakuphanoğlu, S. Altındal, A comparative study on the electrical and dielectric properties of Al/Cddoped ZnO/pSi structures, J. Mater. Sci.: Mater. Electron. 30 (2019) 12122–12129, https://doi.org/10.1007/s10854-019-01570-z.

[14] S. Sonmezoglu, S. Akın, High performance GaAs metal-insulator-semiconductor devices using TiO_2 as insulator layer, Curr. Appl. Phys. 12 (2012) 1372–1377, https://doi.org/10.1016/j.cap.2012.03.030.

[15] J. Chen, J. Lv, Q. Wang, Electronic properties of Al/MoO3/p-InP enhanced Schottky barrier contacts, Thin Solid Films 616 145e150 (2016), https://doi.org/10.1016/j.tsf.2016.08.019.

[16] P. Sumathi, J. Chandrasekaran, R. Marnadu, S. Muthukrishnan, S. Maruthamuthu, J. Mater. Sci.: Mater. Electron. 29 (19) (2018) 16815–16823, https://doi.org/10.1007/s10854-018-9776-7.

[17] Marnadu Raj, Chandrasekaran Joseph, Maruthamuthu Subramanian, Vivek Perumalsamy, Vijayakumar Elayappan, Superior photoresponse MIS Schottky barrier diodes with nanoporous: Sn-WO_3 films for ultraviolet photodetector application, New J. Chem. (2020), https://doi.org/10.1039/D0NJ00101E.

[18] R. Suresh, V. Ponnuswamy, R. Mariappan, N. Senthilkumar, Influence of substrate temperature on the properties of CeO_2 thin films by simple nebulizer spraypyrolysis technique, Ceram. Int. 40 (2014) 437–445, https://doi.org/10.1016/j.ceramint.2013.06.020.

[19] Prakash Chand, Anurag Gaur, Ashavani Kumar, Umesh Kumar Gaur, Structural and optical study of Li doped CuO thin films on Si (1 0 0) substrate deposited by pulsed laser deposition, Appl. Surf. Sci. (2014), https://doi.org/10.1016/j.apsusc.2014.04.027.

[20] M. Uma, V. Rajagopal Reddy, V. Janardhanam, ChelJong Choi, Effect of rareearth Pr6O11 insulating layer on the electrical properties of Au/nGaN Schottky electrode and its chemical and structural characterization, J. Mater. Sci.: Mater. Electron. (2019), https://doi.org/10.1007/s10854-019-02224-w.

[21] K. Mohanraj, D. Balasubramanian, J. Chandrasekaran, Synthesis and characterization of ruthenium-doped CdO nanoparticle and its n-RuCdO/p-Si junction diode application, J. Alloyd Compd. (2018), https://doi.org/10.1016/j.jallcom.2018.11.264.

[22] L. Ben Farhat, M. Amami, E.K. Hlil, R. Ben Hassen, Preparation, X-ray analysis and magnetic investigation of nano structured Co: Yb_2O_3, Mater. Res. Bull. 45 (2010) 1964–1968, https://doi.org/10.1016/j.materresbull.2010.08.007.

[23] Y. Aktas, L. Arda, M. Acikgoz, Z.K. Heiba, S. Aktas, Preparation, growth, and magnetic properties of co-doped Yb_2O_3 nanoparticles and thin films by the sol-gel process, J. Supercond. Nov. Magn. 25 (2012) 2789–2793, https://doi.org/10.1007/s10948-011-1267-5.

[24] P. Vivek, J. Chandrasekaran, R. Marnadu, S. Maruthamuthu, Fabrication of illumination-dependent Cu/p-Si Schottky Barrier diodes by sandwiching MoO_3 nanoplates as an interfacial layer via JNSP technique, J. Electron. Mater. (2020), https://doi.org/10.1007/s11664-020-08137-3.

[25] S. Dolai, R. Dey, S. Das, S. Hussain, R. Bhar, A.K. Pal, Cupric oxide (CuO) thin films prepared by reactive d.c. magnetron sputtering technique for photovoltaic application, J. Alloys Compd. 724 (2017) 456–464, https://doi.org/10.1016/j.jallcom.2017.07.061.

[26] S. Ekambarama, M. Maazab, Combustion synthesis and luminescent properties of Eu^{3+}-activated cheap red phosphors, J. Alloys Compd. 395 (2005) 132–134, https://doi.org/10.1016/j.jallcom.2004.09.075.

[27] P.M. Kibasomba, S. Dhlamini, M. Maaza, C.-P. Liu, M.M. Rashad, D.A. Rayan, B. W. Mwakikunga, Strain and grain size of TiO_2 nanoparticles from TEM, Raman spectroscopy and XRD: the revisiting of the Williamson-Hall plot method, Res. Phys. (2018), https://doi.org/10.1016/j.rinp.2018.03.008.

[28] G.R. Hearne, J. Zhao, A.M. Dawe, V. Pischedda, M. Maaza, M.K. Nieuwoudt, P. Kibasomba, O. Nemraoui, J.D. Comins, Effect of grain size on structural transitions in anatase TiO_2: a Raman spectroscopy study at high pressure, Phys. Rev. B 70 (2004) 134102, https://doi.org/10.1103/PhysRevB.70.134102.

[29] B.T. Sone, E. Manikandan, A. Gurib-Fakim, M. Maaza, Sm_2O_3 nanoparticles green synthesis via Callistemon Viminalis' extract, J. Alloys. Compd. (2015), https://doi.org/10.1016/j.jallcom.2015.07.272.

[30] D. Thangaraju, R. Marnadu, V. Santhana, A. Durairajan, P. Kathirvel, J. Chandrasekaran, S. Jayakumar, M.A. Valentec, Darius C. Greenidgee, Solvent influenced synthesis of single-phase SnS_2 nanosheets for solution-processed photodiode fabrication, Cryst. Eng. Comm. 22 (2020) 525–533, https://doi.org/10.1039/c9ce01417a.

[31] M. Shkir, A. Khan, A.A. Ansari, A.M. El-Toni, I.S. Yahia, M.A. Khan, H. Algarni, S. AlFaify, Facilely fabricated Dy:PbI2/glass thin films and their structural, linear and nonlinear optical studies for opto-nonlinear applications, Vacuum (2019), https://doi.org/10.1016/j.vacuum.2019.109122.

[32] N. Kaymak, E. Efil, E. Seven, A. Tataroğlu, S.B. Ocak, E. Orhan, Effects of temperature and frequency on capacitance and conductance characteristics of zinc-oxide based MIS-Structure, Physica B: Phys. Condensed Matter (2019), https://doi.org/10.1016/j.physb.2019.411721.

[33] K. Kaviyarasu, G.T. Mola, S.O. Oseni, K. Kanimozhi, C.M. Magdalane, M. Maaza, ZnO doped single wall carbon nanotube as an active medium for gas sensor and solar absorber, J. Mater. Sci.: Mater. Electron. 30 (1) (2019) 147–158, https://doi.org/10.1007/s10854-018-0276-6.

[34] Raunak Kumar Tamrakar, Durga Prasad Bisen, Chandra Shekher Robinson, Ishwar Prasad Sahu, Nameeta Brahme, Ytterbium doped gadolinium oxide (Gd2O3:Yb3+) Phosphor: topology, morphology, and luminescence behaviour, Indian J. Mater. Sci. 2014 (2014), https://doi.org/10.1155/2014/396147.

[35] Takayuki Makino, Takaho Asai, Tomoya Takeuchi, Kenichi Kaminaga, Daichi Oka, Tomoteru Fukumura, Temperature dependence of dielectric functions in Yb_2O_3 and Lu_2O_3 epitaxial thin films on sapphire (0001), Jpn. J. Appl. Phys. 59 (2020) SCCB13, https://doi.org/10.7567/1347-4065/ab4a88.

[36] Yasemin Caglar, Müjdat Caglar, Saliha Ilican, Microstructural, optical and electrical studies on sol gel derived ZnO and ZnO: Al films, Curr. Appl Phys. 12 (3) (2012) 963–968, https://doi.org/10.1016/j.cap.2011.12.017.

[37] Cebrail Gumus, Effects of annealing on optical properties of ZnS and ZnS: Mn thin films, J. Optoelectron. Adv. Mater. 12 (2010) 1747–2175.

[38] B.D. Ngom, T. Mpahane, E. Manikandan, M. Maaza, ZnO nano-discs by lyophilization process: size effects on their intrinsic luminescence, J. Alloys Compd. 656 (2016) 758–763, https://doi.org/10.1016/j.jallcom.2015.09.230.

[39] S. Adachi, H. Wakana, M. Horibe, N. Inoue, T. Sugano, K. Tanabe, Preparation of La-doped Yb-123 thin films for high-T_c devices, Physica C 378–381 (2002) 1213–1215.

[40] R. Marnadu, J. Chandrasekaran, S. Maruthamuthu, P. Vivek, V. Balasubramani1, P. Balraju, Jet Nebulizer sprayed WO3nanoplate arrays for highphotoresponsivity based metal–insulator–semiconductor structured Schottky Barrier diodes, J. Inorg. Organomet. Polym Mater. (2019), https://doi.org/10.1007/s10904-019-01285-y.

[41] R. Marnadu, J. Chandrasekaran, M. Raja, M. Balaji, S. Maruthamuthu, P. Balraju, Influence of metal work function and incorporation of Sr atom on WO3 thin films for MIS and MIM structured SBDs, Super Latt. Microstruct. 134 (2018) 119, https://doi.org/10.1016/j.spmi.2018.04.049.

[42] Savita Chaudhary, Sushil Kumar, Ganga Ram Chaudhary, Tuning of structural, optical and toxicological properties of Gd3+ doped Yb2O3 nanoparticles, Ceram. Int. 45 (2019) 19307–19315, https://doi.org/10.1016/j.ceramint.2019.06.181.

[43] A. Büyükbaş Uluşan, A. Tataroğlu, Impedance spectroscopy of Au/TiO_2/n-Si metal-insulator-semiconductor (MIS) capacitor, Physica B: Phys. Condensed Matter (2019), https://doi.org/10.1016/j.physb.2019.411945.

[44] S. Ohmi, C. Kobayashi, I. Kashiwagi, C. Ohshima, H. Ishiwara, H. Iwai, Characterization of La_2O_3 and Yb_2O_3 thin films for high-k gate insulator application, J. Electrochem. Soc. 150 (7) (2003) F134–F140.

[45] V. Balasubramani, J. Chandrasekaran, Tien Dai Nguyen, S. Maruthamuthu, R. Marnadu, P. Vivek, S. Sugarthi, Colossal photosensitive boost in Schottky diode behaviour withCe-V2O5interfaced layer of MIS structure, Sens. Actuators A 315 (2020), https://doi.org/10.1016/j.sna.2020.112333.

[46] A. Tataroglu, S. Altındal, Study on the frequency dependence of electrical and dielectric characteristics of Au/SnO2/n-Si (MIS) structures, Microelectron. Eng. 85 (2008) 1866–1871, https://doi.org/10.1016/j.mee.2008.05.025.

[47] Antonio Di Bartolomeo, Filippo Giubileo, Giuseppe Luongo, Laura Iemmo, Nadia Martucciello, Gang Niu, Mirko Fraschke, Oliver Skibitzki, Thomas Schroeder, Grzegorz Lupina, Tunable Schottky barrier and high responsivity in graphene/Sinanotip Optoelectronic device, 2D Mater. 4 (2017) 015024, https://doi.org/10.1088/2053-1583/4/1/015024.

[48] T.-M. Pan, C.-H. Cheng, C.-D. Lee, Yb_2O_3 thin films as a sensing membrane for pH-ISFET application, J. Electrochem. Soc. 156 (2009) J108–J111, https://doi.org/10.1149/1.3089365.

[49] H. Tanrıkulu, A. Tataroğlu, E.E. Tanrıkulu, A. Büyükbaş Uluşan, Electrical characterization of MIS diode prepared by magnetron sputtering, Indian J. Pure Appl. Phys. 56 (2018) 142–148.

[50] S. Altındal, On the origin of increase in the barrier height and decrease in ideality factor with increase temperature in Ag/SiO2/P-Si (MIS) Schottky Barrier diodes (SBDs), J. Mater. Electron. Dev. 1 (2019) 38–43.

[51] S. Bhuvaneswari, M. Seetha, J. Chandrasekaran, R. Marnadu, High Photoresponsive p-Si/n-In_2O_3 junction diodes with low ideality factor prepared using closely packed octahedral structured In_2O_3 thin films, J. Inorg. Organomet. Polym. Mater. (2020), https://doi.org/10.1007/s10904-020-01663-x.

[52] Adem Tataroglu, Aysel Buyukbas Ulusan, Şemsettin Altındal, Yashar Azizian, A compare study on electrical properties of MS diodes with and without CoFe2O4-PVP interlayer, J. Inorg. Organ. Polym. Mater. 31 (2021) 1–8, https://doi.org/10.1007/s10904-020-01798-x.

[53] S. Altındal Yerişkin, The investigation of effects of (Fe_2O_4-PVP) organic-layer, surface states, and series resistance on the electrical characteristics and the sources of them, J. Mater. Sci.: Mater. Electron. 30 (2019) 17032–17039, https://doi.org/10.1007/s10854-019-02045-x.

[54] R. Siva Prakash, C. Mahendran, J. Chandrasekaran, R. Marnadu, S. Maruthamuthu, Impact of substrate temperature on the properties of rare-earth cerium oxide thin films and electrical performance of p-Si/n-CeO2 junction diode, J. Inorg. Organomet. Polym Mater. (2020), https://doi.org/10.1007/s10904-020-01667-7.

[55] Ç. Bilkan, S. Zeyrek, S.E. San, Ş. Altındal, A compare of electrical characteristics in Al/p-Si (MS) and Al/C20H12/p-Si (MPS) type diodes using current–voltage (I–V) and capacitance–voltage (C–V) measurements, Mater. Sci. Semicond. Process. 32 (2015) 137–144, https://doi.org/10.1016/j.mssp.2014.12.071.

[56] Aysel Buyukbas Ulusan, S. Altındal-Yerişkin, Adem Tataroglu, Forward and reverse bias current–voltage (I–V) characteristics in the metal–ferroelectric–semiconductor (Au/SrTiO3/n-Si) structures at room temperature, J. Mater. Sci.: Mater. Electron. 29 (2018), https://doi.org/10.1007/s10854-018-9767-8.

[57] Şükrü Karataş, The negative capacitance characteristics of in Au/n-GaAs metal-semiconductor contacts at room temperature, J. Mater. Electron. Dev. 4 (2020) 11–13.

[58] Yasemin Şafak Asar, On the temperature dependent reverse current conduction mechanisms in (AuZn)/TiO2/p-GaAs MIS structures, J. Mater. Electron. Dev. 4 (2020) 14–20.

[59] K.S. Mohan, A. Panneerselvam, J. Chandrasekaran, R. Marnadu, Mohd, Shkir, An in-depth examination of opto-electrical properties of In-Y_b2_O3 thin films and fabricated Al/In-Y_b2_O3/p-Si (MIS) hetero junction diodes, Appl. Nanosci. 11 (2021) 1617–1635, https://doi.org/10.1007/s13204-021-01817-4.

[60] Ahmet Faruk Özdemir, Durmuş Ali Aldemir, Ali Kökce, Seçkin Altindal, Electrical properties of Al/conducting polymer (P2ClAn)/p-Si/Al contacts, Synth. Met. 159 (14) (2009) 1427–1432, https://doi.org/10.1016/j.synthmet.2009.03.020.